JOURNAL OF COMPUTATIONAL PHYSICS 56, 203–236 (1984)

A Unified Model for the Evolution of Nonlinear Water Waves

JAMES M. WITTING*

Laboratory for Computational Physics,
Naval Research Laboratory, Washington, D.C. 20375

Received October 12, 1983

Details of a new model of water waves that describes wave propagation over long distances accurately, at low cost, and for a wide variety of physical situations are given. The analysis and numerical methods selected for computer solution are given in some detail. The model uses exact prognostic equations, and a high-order expansion to relate variables at each time step. The accuracy of the model is demonstrated most completely for solitary wave propagation, where model results are compared to exact results. It is found that the model results are much more accurate for high solitary waves than are earlier, Boussinesq-type theories, and give good results for waves so high that they are almost breaking. The capability of the model to treat a variety of situations is demonstrated for colliding solitary waves, nonlinear dispersive wave trains, waves in channels of varying breadth, and undular bores. Formally, the model incorporates nonlinear long wave theory exactly, incorporates enough dispersion to describe linear waves with fourth-order precision, so that both shallow water waves and deep water waves are included, and describes accurately waves for which dispersive and nonlinear effects are both important.

1. INTRODUCTION

Three bodies of theory have long existed that describe the evolution of water waves. *Linear wave theory* treats infinitesimal waves of arbitrary length, and a satisfactory account of the basic theory is available in many places (see, e.g., Lamb [1]). Except at the long wave limit, waves are dispersive, and so only sinusoidal waves of infinite extent can be waves of unchanging shape. *Long wave theory* treats waves infinitely long compared to the depth; they can have arbitrary amplitudes. No wave can propagate with unchanging shape (rates of change of shape tend to vanish in the limit of small amplitudes, or, more precisely, small slope). Waves of depression can be accommodated by the theory for indefinitely long times, but waves of elevation steepen, until at some finite time the horizontal scale at a wave front is not particularly long compared to the depth. Extra features such as bores (the water-wave analog to shock waves in gas dynamics) are added to the long wave theory to complete the description. Again, accounts of the basic theory are widely available (see, e.g., Stoker [2]).

* Present address: ORI, Incorporated, 1375 Piccard Drive, Rockville, Maryland 20850.

0021-9991/84 $3.00

A third situation can exist, in which effects of nonlinearity and dispersion are balanced sufficiently that waves can propagate for long distances without significant change of form, even in the absence of dissipation. The first person to report them in scientific annals was Russell [3, 4]. He first saw a solitary wave in a canal, and being on a horse at the time, was able to chase it along its tow path for a mile or more. He later performed laboratory experiments and reported an accurate relationship between the wave speed and wave amplitude. Much theory has gone into describing such waves, mostly published in two spurts. During the latter part of the nineteenth century the governing equations and some solutions for fairly long waves that can travel both ways (Boussinesq [5, 6]) and one way (Korteweg and deVries [7]) were set down. In their pioneering numerical study of solutions to the Korteweg and deVries (KdeV) equation, Zabusky and Kruskal [8] discovered that overtaking solitary waves emerged with properties no different from their pre-collision ones (apart from roundoff errors and slight phase shifts). They suggested that solitary wave solutions to the KdeV equation be called "solitons" to emphasize their ability to survive nonlinear collisions. Much research on solitons has resulted (see the review by Zabusky [9] for a modern summary).

The word "order" will occur frequently in this paper. Unless qualified, it refers to an ordering of parameters that measure the smallness of wave amplitude and the smallness of wave train dispersion. The lowest order corresponds to long waves of infinitesimal amplitude that travel through water of constant depth. Specifically, at lowest order the wave has an amplitude that is negligible when compared to the undisturbed depth, and any relevant horizontal scale of the wave (wavelength or half-width) is infinitely greater than the undisturbed depth. The waves are non-dispersive. All disturbances can be described as a superposition of waves of unchanging shape. The wave shapes are arbitrary.

The Boussinesq, KdeV, and RLW (regularized long wave—an alternative to KdeV) descriptions each include the lowest-order effects of dispersion and nonlinearity. Each has waves of unchanging shape—solitary waves and periodic waves. Each can describe evolving waves. The accuracies of each description, however, are limited by their retaining only the lowest-order nonlinear and dispersive terms of the governing equations. Numerical models based on these descriptions can be called "*Boussinesq models.*" These include models for one horizontal dimension [10–13] and for two horizontal dimensions [14, 15]. The cost of running the one-dimensional models is small, and the cost of running the two-dimensional models is bearable. The reason for the relatively low cost is the fact that the Boussinesq expansions turn a two-space-dimensions-plus-time-problem into a one-space-dimension-plus-time computer problem.

Other forms of water wave models exist that do not involve a low-order expansion. These include direct numerical solutions of the governing equations of continuity and motion, either in an Eulerian representation [16, 17] or in a Lagrangian representation [18], as well as other methods that offer high resolution of the vertical coordinate [19, 20]. These methods have the capability to solve problems involving breaking waves and other extreme situations that Boussinesq models cannot reach.

Their running costs are high, however, because the problem is essentially that of a two-space-dimensions-plus-time computer problem. Because elliptic equations arise at each time step, and these take fair amounts of computer time, either runs at relatively high resolution for relatively short times are performed, or runs at relatively coarse horizontal resolution are reported.

Some researchers have worked hard on the problem of actual solitary waves in water (restrictions on wave amplitude are removed, dissipation is not treated, and the waves are assumed to be of unchanging shape from the start). These theories produce results on the structure of solitary and periodic waves all the way to breaking, and are excellent benchmarks for assessing the accuracies of theories of waves that evolve to solitary waves [21, 22]. These are special calculations, however, limited to waves of unchanging shape.

This paper describes an extension of Boussinesq-type methodology that is demonstratably accurate for waves where dispersion and nonlinearity are in approximate balance, while still retaining the ability to treat waves where they are not in balance. The analysis retains exactness for as long as is practical. At a crucial step the choice of solving for a flow field by a low-order expansion is made to change the two-dimensional physical problem to a one-dimensional computational problem that can use fast algorithms. This choice limits the description of solitary waves to one order better than the Boussinesq and Korteweg–deVries descriptions (the accuracy turns out to exceed that expected at the same order by comparison with exact solitary wave results). Long wave theory is retained and the linear theory is retained through a high order in a dispersion parameter, and can be extended to even higher orders easily, if desired. The method is straightforward and computationally efficient.

Two distinct elements go into the research: a general mathematical analysis of the physical situation, and a partly empirical formulation of an appropriate numerical method to generate solutions to initital/boundary value problems of interest. Section 2 gives the analytical development. Section 2A discusses the pair of prognostic equations used in the work. One of them comes from recent work [23, 24]. These exact equations do not close the system, however, and expansions are made to close it (Section 2B). In Section 2B the fluid velocity at the bottom boundary is chosen as one of the basic dependent variables to make the expansion far-reaching (for linear waves the expansions converge for all wave numbers). In Section 2C further transformations are made that retain high accuracy while keeping small numbers of terms in the expansions (this is analogous to representing a function by Padé approximants). Section 3 outlines the numerical method used to generate solutions, and discusses boundary and initial conditions. The numerical method is leapfrog, which employs centered time and space finite differences. Its stability properties are discussed. Section 4 describes tests of the accuracy of the model by comparing properties of solitary waves that evolve from the calculation with theories that describe nonevolving solitary waves precisely. The model solitary waves turn out to be surprisingly accurate almost to breaking amplitudes. Section 5 describes the capability of the model to treat a wide variety of physical situations. In (5A) the problem of a head-on collision of solitary waves is examined. The solitary waves are

found to be near-solitons (but not exact-solitons). In (5B) dispersive wave trains are generated to demonstrate how the model handles waves of varying wavelengths. Section 5C shows simulations of laboratory experiments on the propagation of waves through channels of varying breadth. The simulations mirror certain aspects of the experiments that other theories miss. Section 5D shows examples of undular bores running through times and distances long enough to match experiments performed by Favre [25]. Finally, Section 6 discusses the key features of the model that are felt to be chiefly responsible for its accuracy, efficiency, and capability.

2. Analysis

A. *The Exact Governing Equations*

The physical model used here takes the fluid to be incompressible and inviscid, undergoing only irrotational motions. Rigid impermeable walls bound the sides and bottom of the fluid. A constant-pressure surface bounds its top. This physical model is that most frequently taken by other researchers. Figure 1 shows the geometry and the definition of some of the physical variables.

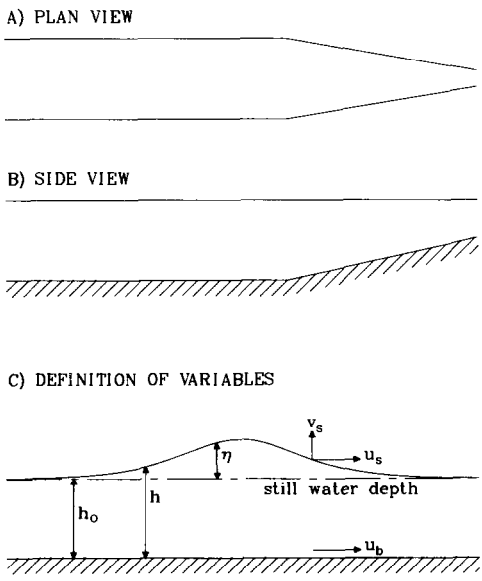

FIG. 1. The geometry of the computational channel. Variable depths as shown in (B) are not treated in this paper.

Three exact relations hold for fluid motions in a channel having breadth b and instantaneous depth h:

$$\frac{\partial \eta}{\partial t} + \frac{1}{b}\frac{\partial}{\partial x}(\bar{u}hb) = 0 \tag{2.1}$$

$$\frac{\partial}{\partial t}(u_s + \eta' v_s) + \frac{\partial}{\partial x}\left[g\eta + \frac{1}{2}(u_s + \eta' v_s)^2 - \frac{1}{2}v_s^2(1+\eta'^2)\right] = 0 \tag{2.2}$$

$$v_s = \frac{\partial \eta}{\partial t} + u_s\frac{\partial \eta}{\partial x} = \frac{1}{1+\eta'^2}\left[\frac{\partial \eta}{\partial t} + (u_s + \eta' v_s)\frac{\partial \eta}{\partial x}\right] \tag{2.3}$$

where the horizontal displacement is x, the time t, the elevation above still water level η, the surface slope η', the components of surface velocity u_s (horizontal) and v_s (vertical), vertically averaged horizontal velocity $\bar{u}$, and the acceleration of gravity g. The vertical coordinate y, positive upwards, does not appear explicitly in (2.1)–(2.3).

Equation (2.1) represents conservation of mass (Stoker [2] gives a complete derivation), and is frequently used by wave modelers. Strictly speaking, the product ηb is the area above still water level and the product $\bar{u}hb$ is the volume flux of fluid. Thus, η should be interpreted as the average elevation above still water level, and $\bar{u}$ as the average horizontal velocity over a cross section. For sidewalls that are close enough together ($b \ll h$), and possibly for wide but gently varying b, η and u are sufficiently constant across the section that η can be taken as the surface elevation and $\bar{u}$ the vertically averaged velocity (see Green [26]). This paper so interprets η and $\bar{u}$, and ignores cross-channel variations throughout.

Equation (2.2) is an unorthodox form of an equation of motion. For irrotational flows $u_s + \eta' v_s$ is just $\partial\phi_s/\partial x$, where ϕ_s is the velocity potential evaluated at the surface. It is a straightforward matter to derive (2.2) from Bernoulli's law. It is used in place of Bernoulli's law here to put it in conservative form. It has more generality than needed here, for it can be derived for inviscid but not necessarily irrotational flows [23]. More recent work interprets the spatial integral of (2.2) as an extension of Kelvin's circulation theorem [24].

Equation (2.3) is the kinematic surface relation. The second identity in (2.3) is a simple (if not transparent) identity.

Letting $q_s \equiv u_s + \eta' v_s$ and substituting (2.3) into (2.2) gives the pair of prognostic equations (in η and q_s) used in the numerical work

$$\frac{\partial \eta}{\partial t} + \frac{1}{b}\frac{\partial}{\partial x}[\bar{u}(h_0 + \eta)\, b] = 0 \tag{2.4}$$

$$\frac{\partial q_s}{\partial t} + \frac{\partial}{\partial x}\left[g\eta + \frac{1}{2}q_s^2 - \frac{1}{2}(1+\eta'^2)^{-1}\left(\frac{\partial \eta}{\partial t} + q_s\eta'\right)^2\right] = 0. \tag{2.5}$$

The term $\partial\eta/\partial t$ in (2.5) can be replaced with a $\partial/\partial x$ term using (2.4) and so each is of the form

$$\frac{\partial f(x,t)}{\partial t}+\frac{\partial g(x,t)}{\partial x}=0 \tag{2.6}$$

where f is either ηb or q_s, and $g(x,t)$ contains η, q_s and $\bar{u}$. Closing the system thus demands that a relation be found connecting η, q_s and $\bar{u}$. This relation is found by considering the velocity potential, which satisfies

$$\nabla^2\phi=0 \tag{2.7}$$

where for irrotational flows

$$u(x,y,t)=\partial\phi/\partial x; \qquad v(x,y,t)=\partial\phi/\partial y. \tag{2.8}$$

B. *A Series Solution*

In terms of the fluid velocity at the bottom (taken here to lie along $y=0$) $u_b\equiv\phi_0'(x,0,t)$, (2.7) gives the Taylor series expansion

$$u(x,y,t)=u_b-\frac{1}{2}u_b''y^2+\frac{1}{24}u_b^{iv}y^4-\cdots+\frac{(-1)^N}{(2N)!}\frac{\partial^{2N}u_b}{\partial x^{2N}}+\cdots \tag{2.9}$$

where primes denote partial differentiation with respect to x.

In terms of u_b, it turns out that

$$\bar{u}=u_b-\frac{1}{6}h^2u_b''+\frac{1}{120}h^4u_b^{iv}-\cdots+\frac{(-1)^N}{(2N+1)!}h^{2N}u_b^{2N\,\text{primes}} \tag{2.10}$$

$$q_s=u_b-\frac{1}{2}(h^2u_b')'+\frac{1}{24}(h^4u_b''')'-\cdots+\frac{(-1)^N}{(2N)!}\frac{\partial}{\partial x}\left(h^{2N}\frac{\partial^{2N-1}u_b}{\partial x^{2N-1}}\right)+\cdots. \tag{2.11}$$

Consequently, both $\bar{u}$ and q_s can be written as functions of u_b. Equations (2.10) and (2.11), along with (2.4) and (2.5), close the system and are an exact representation for irrotational two-dimensional waves in an incompressible inviscid fluid lying atop a rigid impermeable horizontal bed. If the channel walls and/or still water depth vary only gradually over a characteristic distance associated with the wave motion (wavelength or solitary wave thickness, for example) we expect that the set will produce results that are exact in the limit of gradual variation and may be quite accurate for sufficiently gradual variation [26].

C. *Approximations*

In the numerical work (2.4) and (2.5) are used to advance η and q_s by one time level in a finite difference approximation. The problem then arises of how to evaluate the fluxes in the $\partial/\partial x$ terms of (2.4) and (2.5) at this new time level. Using the formulation here, this involves solving (2.11) for u_b from the new values of q_s and $h = h_0 + \eta$. The method of solution adopted here employs a fast "tridiagonal matrix solver." It solves (inverts) matrices containing only on-diagonal and the adjoining off-diagonal elements. Thus, the finite difference form of (2.11) can be inverted if truncated after the term $-1/2(h^2u_b')'$. The resulting formulation would incorporate both long wave theory and Boussinesq theory, but would fail to satisfy the linear water wave theory beyond first order in $k^2h_0^2$. By using the tridiagonal solver repeatedly, and by rewriting the numerical coefficients of the linear terms of (2.10) and (2.11) it is possible to incorporate a long wave expansion of linear wave theory to high order in $k^2h_0^2$ with a minimum number of repeated tri-diagonal solves. This section provides some details that retain second-order accuracy in $k^2h_0^2$ with a single tri-diagonal solve, and fourth-order accuracy with a pair of solves.

The depth h that appears in (2.10) and (2.11) is expressed as $h = h_0 + \eta$. Equation (2.11) is then rewritten

$$q_s = u_b - \tfrac{1}{2}(h_0^2u_b')' - \tfrac{1}{2}[h^2 - h_0^2)\,u_b']' + \cdots. \tag{2.12}$$

A new velocity variable $\tilde{u}$ is then introduced that transforms (2.12) to

$$\begin{aligned} q_s = \tilde{u} &- a_{m,n}^{(1)}(h_0^2\tilde{u}')' - \tfrac{1}{2}[(h^2 - h_0^2)\,\tilde{u}']' \\ &+ a_{m,n}^{(2)}(h_0^4\tilde{u}''')' + \tfrac{1}{24}[(h^4 - h_0^4)\,\tilde{u}''']' - \cdots \end{aligned} \tag{2.13}$$

where $a_{m,n}^{(1)}$ and $a_{m,n}^{(2)}$ are constants that enter the linear terms of (2.13). Equation (2.10) is similarly decomposed, i.e.,

$$\begin{aligned} \bar{u} = \tilde{u} &- b_{m,n}^{(1)}h_0^2\tilde{u}'' - \tfrac{1}{6}(h^2 - h_0^2)\,\tilde{u}'' \\ &+ b_{m,n}^{(2)}h_0^4\tilde{u}^{iv} + \tfrac{1}{120}(h^4 - h_0^4)\,\tilde{u}^{iv} - \cdots. \end{aligned} \tag{2.14}$$

Note that the nonlinear terms in (2.13) and (2.14), those involving h rather than h_0, are unaffected, no matter what the values of the $a_{m,n}$'s and $b_{m,n}$'s.

The coefficients $a_{m,n}$ and $b_{m,n}$ are selected to maximize the accuracy of linear waves. The first few combinations are

1st order:

$$\begin{aligned} &a_{0,1}^{(1)} = 1/3; \qquad a_{0,1}^{(2)} = 0; \cdots \\ &b_{0,1}^{(1)} = 0; \cdots \end{aligned} \tag{2.15}$$

2nd order:

$$\begin{aligned} a_{1,1}^{(1)} &= 2/5; \qquad a_{1,1}^{(2)} = 0; \cdots \\ b_{1,1}^{(1)} &= 1/15; \qquad b_{1,1}^{(2)} = 0; \cdots \end{aligned} \tag{2.16}$$

3rd order:

$$\begin{aligned} a_{1,2}^{(1)} &= 3/7; \qquad a_{1,2}^{(2)} = 1/105; \qquad a_{1,2}^{(3)} = 0; \cdots \\ b_{1,2}^{(1)} &= 2/21; \qquad b_{1,2}^{(2)} = 0; \cdots \end{aligned} \tag{2.17}$$

4th order:

$$\begin{aligned} a_{2,2}^{(1)} &= 4/9; \qquad a_{2,2}^{(2)} = 1/63; \qquad a_{3,3}^{(3)} = 0; \cdots \\ b_{2,2}^{(1)} &= 1/9; \qquad b_{2,2}^{(2)} = 1/945; \qquad b_{2,2}^{(3)} = 0; \cdots . \end{aligned} \tag{2.18}$$

The dispersion relation for linear waves becomes of the form

(1st order)

$$\frac{c^2}{gh_0} = \frac{1}{1 + \frac{1}{3}k^2h_0^2}$$

(2nd order)

$$= \frac{1 + \frac{1}{15}k^2h_0^2}{1 + \frac{2}{5}k^2h_0^2} \tag{2.19}$$

(3rd order)

$$= \frac{1 + \frac{2}{21}k^2h_0^2}{1 + \frac{3}{7}k^2h_0^2 + \frac{1}{105}k^4h_0^4}$$

(4th order)

$$= \frac{1 + \frac{1}{9}k^2h_0^2 + \frac{1}{945}k^4h_0^4}{1 + \frac{4}{9}k^2h_0^2 + \frac{1}{63}k^4h_0^4}.$$

These are the entries to a Padé table $P(N, N)$ or $P(N-1, N)$ representing $\tanh(kh_0)$, and are correct to the order of $k^2h_0^2$ indicated in the parenthesis.

To second order (in dispersion) the calculations can be explained most simply. Use one tridiagonal solve on (2.13),

$$q_s = \tilde{u} - \tfrac{2}{5}(h_0^2\tilde{u}')' - \tfrac{1}{2}[(h^2 - h_0^2)\tilde{u}']', \tag{2.20}$$

thus obtaining $\tilde{u} = \tilde{u}(x, t_{\text{new}})$. Then substitute this value of $\tilde{u}$ into (2.14):

$$\bar{u}(x, t_{\text{new}}) = \tilde{u} - \tfrac{1}{15} h_0^2 \tilde{u}'' - \tfrac{1}{6}(h^2 - h_0^2)\tilde{u}'' \tag{2.21}$$

to evaluate the new value of $\bar{u}$.

If the fields η and q_s are regarded as arising from the dual expansion in an amplitude parameter $\varepsilon \equiv \eta_{\max}/h_0$ and a dispersion parameter $\mu \equiv h_0^2/l^2$, where l is a characteristic horizontal scale of the wave motion, then the procedure using (2.20) and (2.21) retains all terms of the exact equations (2.4) and (2.5) that are the following orders:

$\mu^{1/2}$	(governs waves in long wave theory; if only terms in $\varepsilon\mu^{1/2}$ are retained, we have linear long wave theory)
$\varepsilon\mu^{5/2}$	(an approximation to linear waves)
$\varepsilon^2\mu^{1/2}$ and $\varepsilon\mu^{3/2}$	(the Boussinesq equations retain terms only through these orders)
$\varepsilon^3\mu^{1/2}$; $\varepsilon^2\mu^{3/2}$; $\varepsilon\mu^{5/2}$	(the first order beyond the Boussinesq equations).

The lowest-order terms that are dropped are

$$O(\varepsilon\mu^{7/2}); \qquad O(\varepsilon^2\mu^{5/2}); \qquad O(\varepsilon^3\mu^{3/2}). \tag{2.22}$$

Moving to a 3rd and 4th order formulation, which involves solving (2.13) with 2 successive tridiagonal matrix solvers, pushes the dispersive errors from $O(\varepsilon\mu^{7/2})$ to $O(\varepsilon\mu^{9/2})$ and $O(\varepsilon\mu^{11/2})$, respectively.

Unfortunately, the other terms of (2.22), i.e., $O(\varepsilon^2\mu^{5/2})$ and $O(\varepsilon^3\mu^{3/2})$ remain. Even so, the formulation stands at one order in ε and μ further along than the Boussinesq equations. As we shall see, the numerical results yield solitary waves of a practical accuracy beyond that expected from (2.22).

Figure 2 displays the connection between this theory and other water wave theories. As the figure shows, each theory is valid over a restricted range of nonlinearity, dispersion, or both. The merit of this theory is twofold: first, it incorporates all of long wave theory, no matter how nonlinear, and goes all the way to the fourth order in $k^2h_0^2$ in a long wave expansion of linear theory. Second, this theory goes one order beyond the theories of Boussinesq, Korteweg and deVries, and other investigators who consider nonlinear dispersive waves. Consequently, the formal (and, as will be shown, the practical) accuracy of this theory is higher than the Boussinesq-type theories, and can be applied to higher waves. In summary, this theory can be called a "unified" theory of water wave propagation in that it incorporates long wave theory, a high-order version of linear wave theory, and can treat higher waves than any other time-dependent theory that includes both nonlinearities and dispersion.

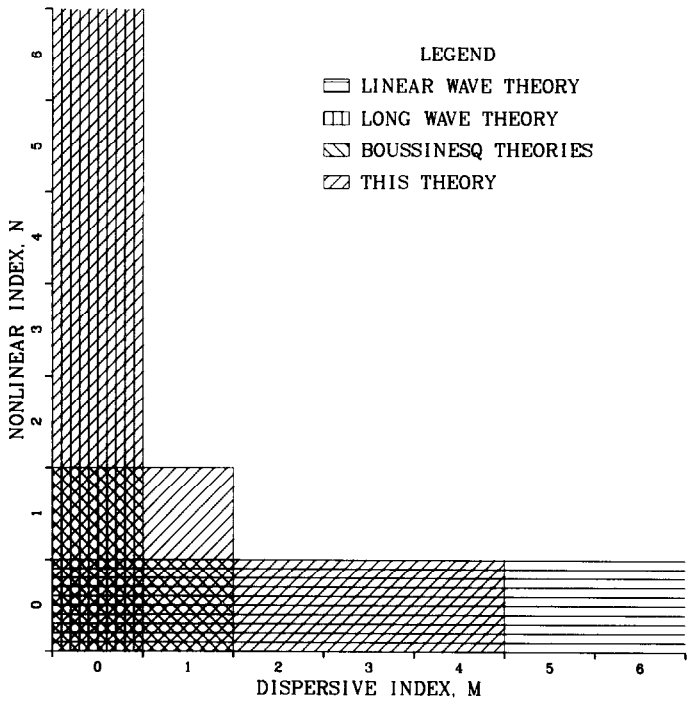

FIG. 2. Various water wave theories for a rectangular channel. Theories of evolving waves in water generally are limited by truncating terms in the exact governing equations that involve dispersion or nonlinearity or both. The convention used here is to consider the linear long wave theory as being of "zeroth" order in dispersion and nonlinearity. The dispersive index M is the power of $(h_0^2 \partial^2/\partial x^2)$ above that of long wave theory. The nonlinear index N is the power of η/h_0 above that of long wave theory. Thus $M=0$ corresponds to $\mu^{1/2}$, $N=0$ to ε^1, $M=N=0$ to $\varepsilon\mu^{1/2}$. Note that for situations where nonlinear and dispersive effects are nearly balanced, this theory extends one order beyond the Boussinesq equations (in each of M, N). For linear dispersive waves this theory (when 4th order coefficients from 2.18 are used) is three orders beyond the Boussinesq equations. This theory recovers long wave theory when $M=0$, unlike some versions of the Boussinesq equations.

To show how well the theory deals with linear waves that are not so long, Fig. 3 gives dispersion relations from various theories. The "2nd order" theory is shown to be fairly accurate. The "4th order" theory that makes use of (2.18) can hardly be distinguished from exact linear theory over the range of kh_0 displayed. This range to $kh_0=8$ takes us into essentially deep water waves. For example, the phase speed of waves having $kh_0=8$ is within 0.0000002 of the speed of waves in infinitely deep water.

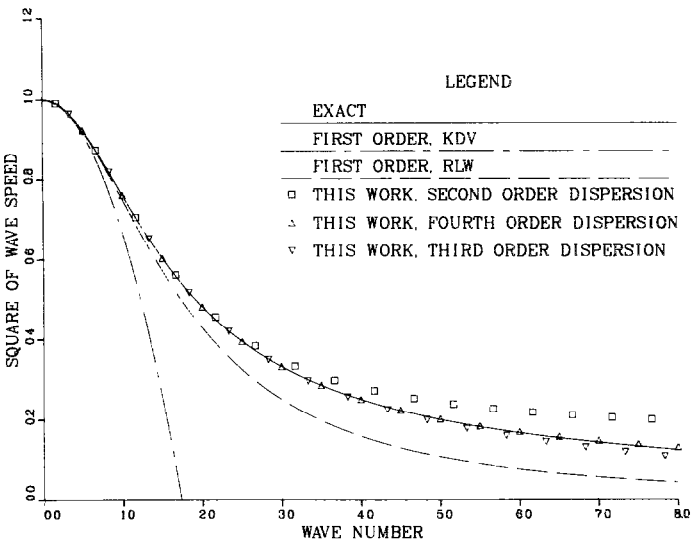

FIG. 3. Dispersion relations for linear water waves.

3. THE NUMERICAL METHOD

A. *The Governing Equations*

The simplest wave problem that the theoretical (and computational) model can address is its lowest-order one—long linear waves in a rectangular channel. Any numerical method used for more complex wave propagation had better do a good job for these. As pointed out earlier, this lowest-order theory retains terms $o(\varepsilon,\mu^{1/2})$ and drops those of higher order. Equations (10)–(11) give $\bar{u}=u_b$; $q_s=u_b$, and so $q\equiv\bar{u}=q_s$ Equations (4)–(5) then become

$$\frac{\partial\eta}{\partial t}+h_0\frac{\partial q}{\partial x}=0 \qquad \text{and} \qquad \frac{\partial q}{\partial t}+g\frac{\partial\eta}{\partial x}=0. \tag{3.1}$$

Systems similar to (3.1) appear in many branches of science. For numerical solution, the unstaggered leapfrog method can be extended to the problem at hand, and can be made accurate by a suitable choice of space and time step. Thus, the approach taken is to represent the fields in finite difference form and approximate derivatives with respect to space and time by central differences.

With subscripts denoting the spatial position, and superscripts the time level, the simplest difference form of (3.1) that places both η and q at the same grid points is

$$\begin{aligned}\frac{\eta_n^{m+1}-\eta_n^{m-1}}{2\Delta t}+h_0\frac{q_{n+1}^m-q_{n-1}^m}{2\Delta x}&=0\\ \frac{q_n^{m+1}-q_n^{m-1}}{2\Delta t}+g\frac{\eta_{n+1}^m-\eta_{n-1}^m}{2\Delta t}&=0.\end{aligned} \tag{3.2}$$

Upon substitution of a linear wave $\propto \exp i(\omega t - kx)$ for η and q we derive

$$\frac{\sin^2(\omega \Delta t)}{(\Delta t)^2} = g h_0 \frac{\sin^2(k\Delta x)}{(\Delta x^2)}. \tag{3.3}$$

Equation (3.3) is neutrally stable for $|\Delta t| \leqslant |\Delta x| (g h_0)^{-1/2}$, in that ω is real for all real k. The dispersion relation for $\Delta t = \Delta x (g h_0)^{-1/2}$ is

$$\omega^2/k^2 = g h_0 \tag{3.4}$$

which is exact for arbitrary wave numbers and numerical resolution Δx. When $|\Delta t| \neq |\Delta x| (g h_0)^{-1/2}$, we can derive the relation

$$\frac{\omega^2}{k^2 g h_0} = 1 - \frac{k^2}{3} [(\Delta x)^2 - g h_0 (\Delta t)^2] + O[(\Delta x/h_0)^4]. \tag{3.5}$$

This equation contains second-order numerical dispersion unless $|\Delta t| = (g h_0)^{-1/2} |\Delta x|$. It thus appears that the choice of $|\Delta t| = (g h_0)^{-1/2} |\Delta x|$ will likely minimize numerical dispersion for fairly long waves. For long linear waves this choice lies at the boundary of instability, however, and we must examine stability in a little detail for the more general problem. To do this, let us consider the effects of nonlinearity and dispersion separately.

Consider dispersion first. The second-order linear set of equations takes the dimensionless form

$$\begin{aligned} &\frac{\partial \eta}{\partial t} + \frac{\partial \tilde{u}}{\partial x} - \frac{1}{15} \frac{\partial^3 \tilde{u}}{\partial x^3} = 0 \\ &\frac{\partial}{\partial t} \left[\tilde{u} - \frac{2}{5} \frac{\partial^2 \tilde{u}}{\partial x^2} \right] + \frac{\partial \eta}{\partial x} = 0. \end{aligned} \tag{3.6}$$

Distances are measured in units of h_0 and speeds in units $\sqrt{g h_0}$. Again, letting the field be represented as proportional to $\exp[i(\omega t - kx)]$, we can derive

$$\sin^2(\omega \Delta t) = \left(\frac{\Delta t}{\Delta x} \right)^2 \sin^2(k\Delta x) \left\{ \frac{1 + \frac{2}{15} P}{1 + \frac{4}{5} P} \right\} \tag{3.7}$$

where $P = [1 - \cos(k\Delta x)]/(\Delta x)^2 \geqslant 0$. Consequently, the expression within the brackets of (3.7) never exceeds unity. For $(\Delta t/\Delta x)^2 \leqslant 1$, the RHS of (3.7) does not exceed unity, so ω is real, i.e., we again have neutral stability for all k, Δx.

After expanding (3.7), one can derive the numerical dispersion relation (for $|\Delta t| = |\Delta x|$)

$$\omega^2 = k^2 \frac{1 + \frac{1}{15} k^2}{1 + \frac{2}{5} k^2} + \frac{1}{36} k^4 (\Delta x)^2 + \text{higher-order terms in } (\Delta x)^2. \tag{3.8}$$

The first term of the right-hand side of (3.8) gives the exact dispersion relation for (3.6). The lowest-order numerical dispersion errors are proportional to $k^4(\Delta x)^2$, with a small coefficient, in contrast to a choice $|\Delta t| < |\Delta x|$, which would introduce an error $O[k^2(\Delta x)^2]$ with a not-so-small coefficient unless Δt is almost Δx.

Other formulations of the problem, besides being of lower order, sometimes choose a velocity variable in such a way that (accidentally) constrains practical solutions. For example, if q_s (the same as u_s in the low-order formulation) is taken to be the dependent velocity variable, the linearized Boussinesq equations are still in the form of (3.6), but with $\tilde{u}$ replaced by q_s and different numerical coefficients: in (3.6), $-1/15$ goes to $+1/3$ and $2/5$ goes to zero. Then (3.7) becomes

$$\sin^2(\omega\Delta t) = \left(\frac{\Delta t}{\Delta x}\right)^2 \sin^2(k\Delta x)\left\{1 - \frac{2}{3}P\right\}. \tag{3.9}$$

Here the factor within the brackets approaches $-\infty$ as $(\Delta x)^2 \to 0$, and so $\sin^2(\omega\Delta t) < 0$ and ω can have an imaginary part, presumably unstable. Only if Δt goes to zero at least as fast as $(\Delta x)^3$ is stability assured. This makes numerical work very expensive for equations having more dispersion in forms like the first of (3.6) than in forms like the second, because more time steps must be taken. The Korteweg–deVries equation has expensive dispersion, and typical finite difference solutions even as coarse as $\Delta x = 0.25$ require time steps the order of 10^{-4} (See Vliegenthart [27] for fuller discussion). The regularized long wave equation, on the other hand, has its dispersion in a form akin to the second of (3.6), and numerical work can be done at $\Delta t = \Delta x$ (e.g., Bona *et al.* [28]).

The inclusion of some nonlinear terms to (3.6) for simple waves changes the stability analysis only by a little when the waves are long. Then one can approximate the nonlinear terms as the product of a slowly varying field and a potentially unstable rapidly varying field. The slowly varying field is incorporated in the long wavelength wave speed, resulting in

$$\sin^2(\omega\Delta t) = \left(\frac{c\Delta t}{\Delta x}\right)^2 \sin^2 k\Delta x \left\{\frac{1 + \frac{2}{15}P}{1 + \frac{4}{5}P}\right\} \tag{3.10}$$

where $c = (gh)^{1/2} \pm u$ includes nonlinear contributions and can exceed unity. Thus $(c\Delta t/\Delta x)^2$ is a factor that can exceed unity when $\Delta t = \Delta x$. Note, however, that this does not imply instability, for $\sin^2(k\Delta x)\{(1 + \frac{2}{15}P)/(1 + \frac{4}{5}P)\}$ is bounded by a number less than unity, the bound being dependent on $(\Delta x)^2$. For example, for $\Delta x = 1/8$, typical of the computations run to date, this factor never exceeds 0.2. Hence, c can exceed unity by a comfortable margin without necessarily giving instabilities. The stability analysis given here is not complete, however. Computational instability has arisen for some cases involving very high waves. The conditions under which instability occurs will be identified later.

B. *Boundary Conditions*

In all calculations run to date, rigid impermeable side and end walls bound the fluid. For Laplace's equation (2.7) to possess valid solutions we must specify a local property of ϕ everywhere along a closed boundary. Here the boundary conditions at the lower boundary are specified by the form of (2.9). The top boundary condition is specified by (2.5) which says, in essence, that the pressure is constant there. At the ends the physics demands that the normal components of fluid velocity match the wall velocity at each point. This can be transformed to conditions on η and q_s demanded by this formulation. Taking walls to be vertical and moving horizontally,

$$u(\text{wall}, y, t) = U(t) \tag{3.11}$$

where $U(t)$ is the wall speed.

We further need a condition on η at the wall. This is most easily derived in a Lagrangian formulation. One equation of motion is

$$\frac{\partial^2 x(a, b, t)}{\partial t^2}\frac{\partial x}{\partial a} + \left[\frac{\partial^2 y(a, b, t)}{\partial t^2} + g\right]\frac{\partial y}{\partial a} + \frac{1}{\rho}\frac{\partial p(a, b, t)}{\partial a} = 0 \tag{3.12}$$

where a and b are the initial coordinates of the fluid particle now at (x, y). Let us evaluate the terms for the fluid surface particle at the wall. When the wall is nonaccelerating the first term vanishes. When the fluid surface is horizontal at the initial time, the third term vanishes. Apart from the possibility that the fluid at the surface accelerates at exactly $-g$, this demands that $\partial y/\partial a = 0$, which is the same as

$$\frac{\partial \eta}{\partial x} = 0. \tag{3.13}$$

We know that u_s (wall, t) $= U$. Using (3.11)

$$q_s = U \tag{3.14}$$

at the wall, so long as it is nonaccelerating. We do not consider accelerating end walls in this report.

C. *Initial Conditions and Time Levels*

All calculations are started by specifying the wall geometry and values of $\eta(x, t = 0)$, $q_s(x, t = 0)$ throughout the region. From these one calculates $\tilde{u}$ from (2.13) and $\bar{u}$ from (2.14) at $t = 0$. Values of η and q_s at $t = \pm(1/2)\,\Delta t$ are formed by one-sided time differencing and the fluxes entering (2.10) and (2.11) at $t = +(1/2)\,\Delta t$ are found. The fields at $t = -(1/2)\,\Delta t$ and fluxes at $t = +(1/2)\,\Delta t$ are used to advance the calculation to $t = (3/2)\,\Delta t$. Fluxes at $t = (3/2)\,\Delta t$ and fields at $t = (1/2)\,\Delta t$ are used to advance to $t = (5/2)\,\Delta t$ and the process is repeated indefinitely. For some runs the process is continued to $t = (N + (1/2))\,\Delta t$, and then the time interval is

reversed, i.e., $dt \to -dt$, using the fields at $t = (N + 1/2)\Delta t$ as initial conditions. The time levels on the return toward $t = 0$ are $t = N\Delta t$, and lie midway between the advancing-time levels until $t = 0$ is reached.

There appears to be some advantage in the procedure of initially moving to two adjacent time levels symmetrically. Other procedures such as a forward or backward whole time step difference gave some alternating grid point noise which, of course, the pure leapfrog method does not suppress as time advances. Trapezoidal corrections to the leapfrog method suppress this oscillation, but also damp waves a little and decrease the accuracy of solitary waves. I have seen no evidence of statistically significant alternating grid point noise in the the fields when the calculations are started symmetrically, as described above.

4. Tests of the Accuracy and Stability of the Calculations

A series of runs were made in a long channel of uniform breadth with initial conditions

$$\eta(x, t = 0) = q_s(x, t = 0) = a_i \operatorname{sech}^2 \alpha(x - x_{\max}) \tag{4.1}$$

where a_i is an initial amplitude, and α is related to it by

$$\alpha = \tfrac{1}{2}\sqrt{3a_i/(1 + a_i)}. \tag{4.2}$$

The relation between η and q in (4.1) and between α and a_i in (4.2) holds for the (lowest order) analysis of a solitary wave found in Lamb [1]. The computational box contained 1840 grid points; time was advanced through 1184 time steps. The step sizes were $\Delta x = \Delta t = 1/8$, so that the box length is approximately $L = 230$, and time advanced to approximately 148. Some nonsolitary wave disturbance was present in the initial conditions for all runs, but the solitary wave soon outran other disturbances.

Various diagnostics were performed to determine the properties of this wave. The location and value of the crest elevation was found by fitting a parabola through the highest elevation and its neighbors, from which a wave speed was determined. Various integral properties of the solitary wave, such as its mass, $2\int_{\eta_{\text{crest}}}^{\infty} \eta\, dx$, were determined by numerical integration from the crest to the right side of the box. The two linear conserved quantities in (2.4) and (2.5), mass and velocity, are found to be conserved properly in the calculations.

Specifically, from (2.4) the conserved quantity is the total area above still water level; this comes from multiplying (2.4) by b and integrating over the computational box

$$\frac{\partial}{\partial t}\int_{x_{\text{left}}}^{x_{\text{right}}} (\eta b)\, dx + [\bar{u}(h_0 + \eta)\, b]|_{x_{\text{right}}} - [\bar{u}(h_0 + \eta)\, b]|_{x_{\text{left}}} = 0. \tag{4.3}$$

Because $\bar{u} = 0$ at the end walls, x_{right} and x_{left}, only the first term of (4.3) is nonzero. Integration over time gives

$$\int_{x_{\text{left}}}^{x_{\text{right}}} (\eta b)\, dx = \text{Const.} \tag{4.4}$$

The integral of (4.4) is monitored at each step of the calculation, and is found to be constant (to the four significant figures printed out in every calculation). From (2.5) the conserved quantity is an integral of q_s, i.e.,

$$\frac{\partial}{\partial t}\int_{x_{\text{left}}}^{x_{\text{right}}} q_s dx + \left[g\eta - \frac{1}{2}\left(\frac{\partial \eta}{\partial t}\right)^2 \right]\Bigg|_{x_{\text{right}}} - \left[g\eta - \frac{1}{2}\left(\frac{\partial \eta}{\partial t}\right)^2 \right]\Bigg|_{x_{\text{left}}} = 0 \tag{4.5}$$

where in (4.5) we have dropped terms involving q_s and η' at the ends, because they vanish there. The integral over time produces

$$\int_{x_{\text{left}}}^{x_{\text{right}}} q_s\, dx = -\int_{t=0}^{t} \Bigg\{ g(\eta_{\text{right}} - \eta_{\text{left}}) - \frac{1}{2}\left[\left(\frac{\partial \eta_{\text{right}}}{\partial t}\right)^2 - \left(\frac{\partial \eta_{\text{left}}}{\partial t}\right)^2 \right] \Bigg\} dt + \text{Const.} \tag{4.6}$$

Equation (4.6) says that at each time the total "velocity" in the box $\int q_s\, dx$ varies only by fluxes entering from the end walls (the right-hand side of (4.6)). Before disturbances reach the walls we find that $\int q_s\, dx$ is conserved to four significant figures. After $\eta \neq 0$ at an end wall, we find the differences between the two sides of (4.6) are small and can be explained as roundoff and truncation errors.

Figure 4 shows the wave speed, Fig. 5 the total solitary wave mass, and Fig. 6 the total energy of the solitary wave. The squares represent runs with second-order dispersion (see 2.16); the triangles represent third-order and fourth-order dispersion runs (2.17 and 2.18). Because these are solitary waves, where nonlinear effects balance dispersive ones, the formal accuracy of the analysis on which the computations are based is limited to second order, however, and improving the dispersive contribution alone should not effect the formal accuracy of the solutions. From Figs. 4–6 it is clear that the numerical calculations are accurate—more so than "second-order" solitary wave theories. The second-order dispersion gives the most accurate results, likely a fortuitous result, and one which I do not emphasize. No matter how the dispersion is treated, the solitary waves are accurate. The highest run using second-order dispersion shown in the figures occurs when in (4.1) $a_i = 0.5$, giving a wave that asymptotically has an amplitude of 0.5853. When $a_i = 0.6$ was attempted, the calculations became unstable. Using fourth-order dispersion, $a_i = 0.6$ leads to a wave having an amplitude of 0.724. The run for $a = 0.7$ became unstable. No attempts at finding out where runs with third-order dispersion became unstable were made.

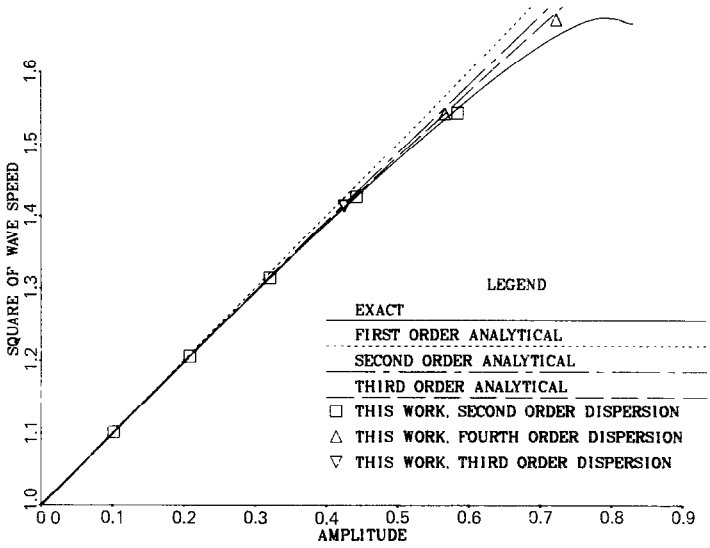

FIG. 4. Comparison of solitary wave speeds. The exact results are from Longuet–Higgins and Fenton [21] and from Witting [22]. The analytical expansions are from Longuet–Higgins and Fenton [21]. The first-order wave speed retains terms through (a/h_0), the second through $(a/h_0)^2$, etc. All computations here are made with $\Delta x = \Delta t = 1/8$.

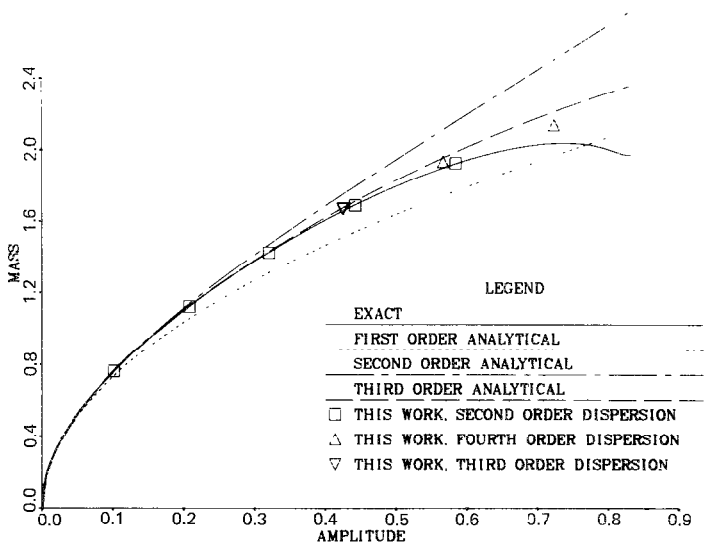

FIG. 5. Comparison of solitary wave masses. The exact results are from Longuet–Higgins and Fenton [21] and from Witting [22]. The analytical expansions are from Longuet–Higgins and Fenton [21]. The first order mass retains terms through $(a/h_0)^{1/2}$, the second through $(a/h_0)^{3/2}$, etc. All computations here are made with $\Delta x = \Delta t = 1/8$.

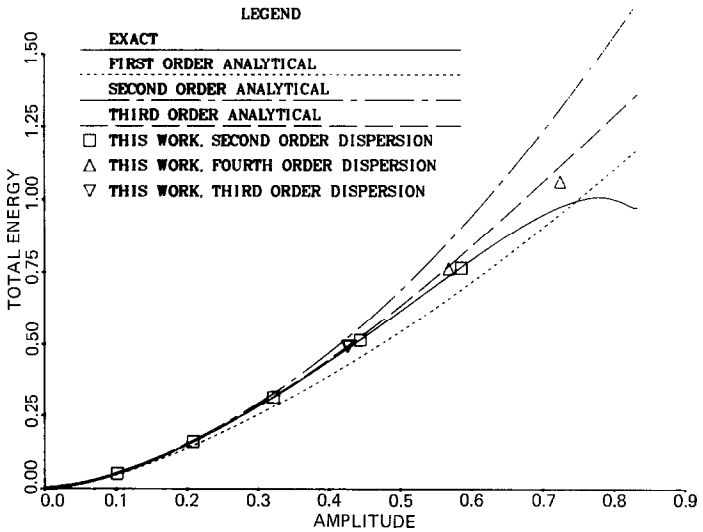

FIG. 6. Comparison of solitary wave energies. The exact results are from Longuet–Higgins and Fenton [21] and from Witting [22]. The analytical expansions are Longuet–Higgins and Fenton [21]. The first-order energy retains terms through $(a/h_0)^{3/2}$, the second order through $(a/h_0)^{5/2}$, etc. All computations here are made with $\Delta x = \Delta t = 1/8$.

The resolution $\Delta x = \Delta t = 1/8$ is sufficient to make truncation errors small. Results at resolution $\Delta x = \Delta t = 1/4$ show slight departures from those displayed. Runs at $\Delta x = \Delta t = 1/16$ are unstable at lower amplitudes than at $\Delta x = \Delta t = 1/8$. This result may be caused by roundoff error, and might not hold for calculations carried out with more precision than the 6–7 places used (single precision). Where results of runs using $\Delta x = \Delta t - 1/8$ and $\Delta x = \Delta t = 1/16$ can be compared, they agree within roundoff errors. This is in accordance with the linear analysis leading to Eq. (3.8), for $(1/36)\, k^4(\Delta x)^2$ is very small, even if the estimate of appropriate values to use for k^4 are not so small. If we assume that truncation errors are proportional to $(\Delta x)^2$, the small differences observed between a run with $\Delta x = 1/4$ and $\Delta x = 1/8$ indicate that truncation differences between runs with $\Delta x = 1/8$ and $\Delta x = 1/16$ should be masked by roundoff error, as observed.

5. EXAMPLES

While it is not difficult to run numerous examples of water waves that have different boundary geometries and initial conditions, this paper limits discussion to

solitary waves colliding head-on is shown. In B examples of essentially dispersive wave trains are shown. In C examples of solitary waves propagating in a converging/diverging channel are shown. In D an example of long waves of depression coupled

with an undular bore is shown. These examples are designed to illustrate the capability of the numerical calculations to treat waves for which dispersive effects are larger than, less than, and comparable to nonlinear effects.

A. *Solitary Wave Collision*

The past twenty years has witnessed a surge of interest in whether the solitary waves described by various model equations are solitons. Here I define solitons as solitary waves that emerge from a collision with each other having the identical structure that they had prior to colliding (an individual soliton may be retarded or advanced during the collision). The two first-order theories that have been used to study colliding solitary waves in water are the Korteweg–deVries equation

$$\frac{\partial \eta}{\partial t}+\frac{\partial \eta}{\partial x}+\frac{3}{2}\eta\frac{\partial \eta}{\partial x}+\frac{1}{6}\frac{\partial^3 \eta}{\partial x^3}=0 \tag{5.1}$$

and the regularized long wave equation

$$\frac{\partial \eta}{\partial t}+\frac{\partial \eta}{\partial x}+\frac{3}{2}\eta\frac{\partial \eta}{\partial x}-\frac{1}{6}\frac{\partial^3 \eta}{\partial x^2\,\partial t}=0. \tag{5.2}$$

The formal accuracies of (5.1) and (5.2) are the same. The first two terms are $O(\varepsilon\mu^{1/2})$, the next is $O(\varepsilon^2\mu^{1/2})$ and the last is $O(\varepsilon\mu^{3/2})$. At $O(\varepsilon\mu^{1/2})$ the solution is $\partial/\partial t=-\partial/\partial x$, so that in the last term of (5.1) $-\partial/\partial t$ may be substituted for $\partial/\partial x$ to give (5.2) without modifying the formal accuracy. Yet the solitary waves of (5.1) are solitons (Zabusky and Kruskal [8]), while those of (5.2) are not quite solitons (Bona *et al.* [28], Santarelli [29], Lewis and Tjon [30].

Here I describe calculations designed to see whether solitary waves in the higher-order theory are solitons. The still water depth and the breadth of the channel are constant. The initial form of each wave is chosen to have a waveform that is solitary-wave-like, i.e.,

$$\eta = a\,\mathrm{sech}^2\,\alpha(x-x_{\max}) \tag{5.3}$$

where $x_{\max}$ marks the initial location of a wave crest, and a and α are adjustable parameters, as in Eq. (4.1). After some experimentation, I have found that the choice of a and α that produces acceptably small disturbances other than a propagating solitary wave differs a little from that of (4.2). Here a solitary wave is chosen having one of the amplitudes listed in Longuet–Higgins and Fenton [21, Table 5], for which selected, essentially exact, solitary wave properties are known. Among these are the speed , the mass $\int_{-\infty}^{\infty}\eta\,dx$, and the potential energy $\frac{1}{2}\int_{-\infty}^{\infty}\eta^2\,dx$. These latter two are sufficient to determine a and α for the particular solitary wave in mind. The initial value of q_s is found by setting $\partial/\partial t=\pm F\,\partial/\partial x$ in (2.5) [the $-$ sign for an intended right-going wave and the $+$ sign for left-going], and solving the resulting quadratic equation for $q_s=q_s(F,\eta,\eta')$.

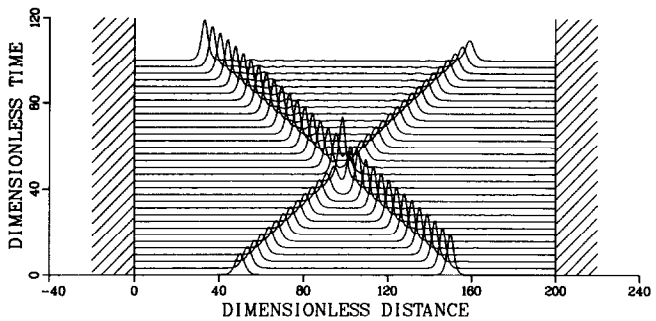

FIG. 7. Space-time display of the elevation above still water level of two solitary waves colliding head-on. The amplitudes of the waves are initially 0.2 and 0.4. The time interval between curves is 3.125. The calculations are run with second order dispersion and $\Delta x = \Delta t = 1/8$.

Figure 7 shows plots of the elevation above still water of a disturbance which started with a pair of solitary-like waves. The wave initially at $x = 50$ approaches an amplitude of 0.1970 prior to the collision. The wave initially at $x = 150$ approaches an amplitude of 0.3861 before the collision. During the collision the elevation reaches 0.6350, somewhat more than the sum of the amplitudes of the colliding waves. By the end of the experiment the rightward wave had reached an amplitude of 0.1962 (and was still rising slowly), and the leftward wave had reached an amplitude of 0.3851 (and was also still rising).

Figure 8 takes the same data as used to plot Fig. 7, expands vertical scales by a factor of 3 and clips off the wave crests. Although some oscillatory wave trains are visible that have their origin at the initial condition, the major oscillatory wave trains that fill the region between the solitary waves at $t \gtrsim 50$ emanate from the collision. These waves have some energy that the solitary waves are leaving behind. Consequently, the solitary waves cannot be solitons (strictly speaking, no more than one of them can be).

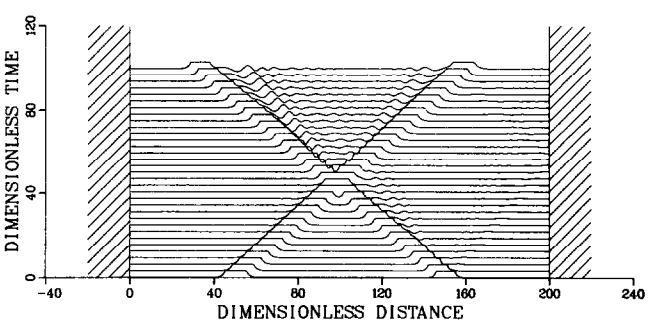

FIG. 8. Expanded view of the solitary wave collision of Fig. 7. Vertical scales are enhanced by a factor of three and large elevations are clipped at the value 0.02.

The question remains whether the existence of the oscillatory wave trains that show the solitary waves to be not exactly solitons can be an artifact of the finite difference numerical treatment. One potential source of error could be what numerical analysists refer to as truncation error, which tends to be proportional to $(\Delta x)^2$ for small Δx. To rule out this possibility, the calculations were run with $\Delta x = \Delta t = 1/4$. i.e., at one half the resolution of Figs. 7–8. The oscillations between the solitary waves had about the same amplitudes and phases at both numerical resolutions. For example, the first few minima and maxima to the right of the larger solitary wave at the top of Figs. 7–8 have the values −0.0092, +0.0096, −0.0068, +0.0034, −0.0047, +0.0047. The coarser resolution run gives the corresponding values of −0.0087. +0.0127, −0.0078, +0.0083, −0.0062, +0.0071. While it is true that the coarser resolution oscillations are a little more intense than the finer resolution ones, they are not the factor 4 expected under the hypothesis that the existence of the oscillatory train is due to truncation error (the reason the oscillations are a little stronger is likely due to the fact that with the same initial conditions the solitary waves are a little higher before collision for $\Delta x = \Delta t = 1/4$, than for $\Delta x = \Delta t = 1/8$).

To see whether the treatment of dispersive terms would influence the propagation, a run at $\Delta x = \Delta t = 1/8$ with fourth order dispersion (not the second order for Figs. 7 − 8) was made. Again, the oscillatory wave train is present, with almost exactly the same amplitudes and nearly the same location of maxima and minima as in Figs. 7–8.

Finally, a test was made to see whether any diffusive artifacts were introduced into the computer program. Figure 9 shows the results of a calculation run to a time of 100, then time reversed. This involves a total of 1600 time steps. (As for Fig. 8, the

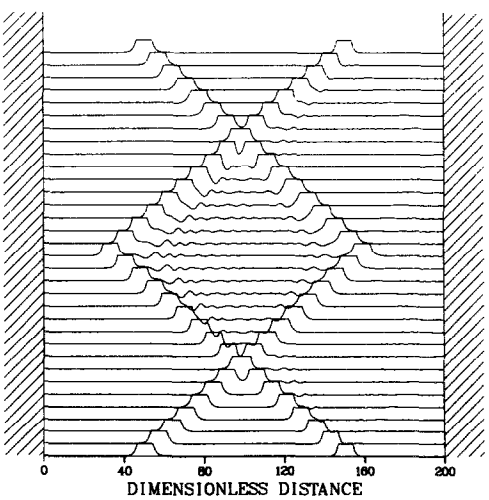

FIG. 9. Expanded view of the same solitary wave collision, but with time reversal and clipping at 0.04. The time scale is the same as for Figs. 7–8, so that the time interval between curves is 6.25.

amplitudes are clipped). To be scale of the figure the calculations are perfectly reversible. The uppermost profile shown in Fig. 9 would be identical to the initial profile if the calculations were perfectly reversible. In fact, these two differ by $O(10^{-4})$ throughout the computational region. We ascribe these small differences to roundoff error in running through 1600 time steps (800 forward and 800 back) with single-precision accuracy (6–7 significant figures). The phases of the crests are remarkably well preserved. For example, the crest of the leftward propagating wave, which started at $x = 150.000$ returned to $x = 150.015$, after the round trip travel distance of 234. We may conclude that these colliding solitary waves are almost solitons, but not quite.

B. *Dispersive Wave Trains*

The wave model derived here is designed to produce solutions for linear and not so linear wave trains that are not necessarily long. To see how faithfully the model represents such wave trains, consider the disturbance produced from the initial condition

$$\eta = 0.08(x - 25)\,\mathrm{sech}^2\, 0.08(x - 25)$$
$$q = \eta. \tag{5.4}$$

The nondimensionalization is again the obvious $h_0 = g = 1$. This type of disturbance resembles that of an impulse distributed over a spatial region of the order of unity. Figure 10 shows the results of the calculations running for a non-dimensional time of 100 and time reversed for the following time interval of 100 (1600 time steps in all). The result is a dispersive wave train. The longer waves travel faster than the shorter ones, and so these longer waves appear at the front of the train. As in all of the figures in this paper, the time and space scales are set so that a feature of a disturbance (a crest, for example) lines up with a slope of exactly unity if it travels with a speed of unity (in dimensionless units; unity corresponds to the long wavelength limit of linear wave propagation, $\sqrt{gh_0}$ in dimensional units). As Fig. 10 shows, the longer waves at the front of the train have speeds slightly less than unity, while the shorter waves travel slower. Waves near the rear of the train are very short, having length scales considerably less than the depth. (The best measure of a length scale of a periodic wave is its inverse wave number κ^{-1}, rather than its wavelength λ. This makes the measure of the smallness of the wave scale equal to kh_0, a number that is unity when the waves are intermediate between being shallow water waves deep water waves. In Fig. 10 the waves near the back of the forward going train are essentially deep water waves.) Thus, the wave model sees essentially deep water waves, even though its design involves an expansion in a parameter that vanishes only in the limit of shallow water waves. How well the model treats deep water waves is still a matter of conjecture, because sufficient testing has not yet been performed. It is comforting, however, that we see the deep water waves, and the dispersion relations shown in Fig. 3 say that waves should be pretty well represented out to kh_0 as large as 8 or more (these are really deep water waves).

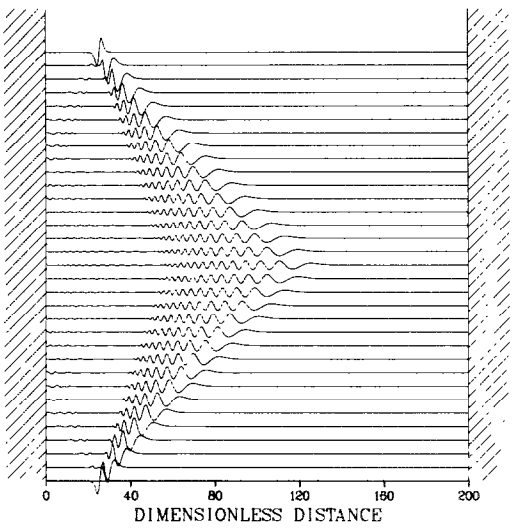

FIG. 10. Waves from an impulse-like initial waveform, with time reversal. The time scale is the same as the space scale, so that the time interval between profiles is 6.25 and speeds of ± 1 would show up along lines oriented at $\pm 45°$. Time advances to $t = 100$, and receeds to $t = 200$. The elevation scale is 0.05 per interval: the initial waveform has a maximum of a little less than 0.05. The calculations are run with second-order dispersion and $\Delta x = \Delta t = 1/8$.

As in the calculations that produce Fig. 9, the code is reversible, apart from round-off error. The topmost profile is identical to the initial lowermost profile to within a few parts in 10^{-6}. The maximum elevation of the topmost profile occurs at the location $x = 25.966$, where it was initially at 25.965, thus indicating very good phase stability.

In order to make more quantitative statements about how well the model handles dispersive wave trains, calculations were performed with the initial profile

$$\eta = 0.5 \operatorname{sech}^2 0.2(x - 12.5) \cos 2(x - 12.5) \tag{5.5}$$

and the initial surfaces velocity set from using (2.5), with F being the anticipated wave speed of a periodic wave having wave number 2.0. The resulting disturbance is almost entirely right-going, as expected. Figure 11 shows 33 profiles, equally spaced in time, running from $t = 0$ to $t = 50$. Both an individual wave crest and the entire disturbance travel at speeds less than unity. The crests travel faster than the group, entering at the left and disappearing at the right. This is a graphic demonstration that for water waves the phases travel faster than the group.

The computational data that make up Fig. 11 were examined in some detail. To round-off error, the largest wave crest travels at the linear speed of waves of wave number 2.0. Again to round-off error, the entire group travels at the group speed of linear waves. This latter result is not surprising, even though the wave train is so

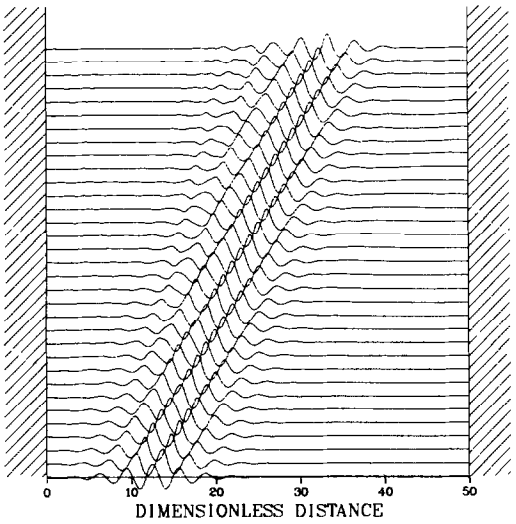

FIG. 11. Dispersive wave packet. The time scale is the same as the space scale, so that the time interval between profiles is 1.5625. The elevation scale is 0.15 per interval; the intital waveform has a maximum of 0.15. Calculations are run with fourth-order dispersion and $\Delta x = \Delta t = 1/8$.

short that the notion of a group speed (in the linear theory) is a little fuzzy. The former result, that the phase of the largest wave traveled at the *linear* phase speed, surprises me a little. Because the waves near the center of the train are not small-amplitude, one might expect that they would move with speeds a little larger than the predictions of linear theory. For example, the crest of a nonlinear periodic wave described by Stokes wave theory should travel approximately 4.4 percent faster than linear waves of the same wavelength for the example shown. The precision of the calculations of crest speed is about 0.5 percent. Why the largest crest travels closer to what linear theory predicts, rather than what nonlinear theory predicts, is an unanswered question at this time. It may have to do with the shortness of the train, so that the largest crest is intimately connected with small amplitude waves; more likely, the fact that at $k = 2.0$ the waves are closer to being deep water waves than shallow water waves means that accuracies of the model are no better than a linear wave model (see Fig. 2).

As a test of one aspect of the model, the data used in generating Fig. 11 were examined a little more carefully to see whether one feature of high, not-so-long waves that is obvious to any observer of waves—their sharp-crestedness— becomes more apparent as the wave amplitude increases. The waves of Fig. 11 are more nearly deep-water waves than shallow-water waves, and their slope is the better measure of nonlinearity than their amplitude-depth ratio. Here the maximum slope is about 0.3, and so the waves are not "small amplitude"; they are also not "near-breaking," which would call for maximum wave slopes of the order of 0.6 (tan 30°). Figure 12 is a blowup of the data from the uppermost profile of Fig. 11 (at the top) and of the

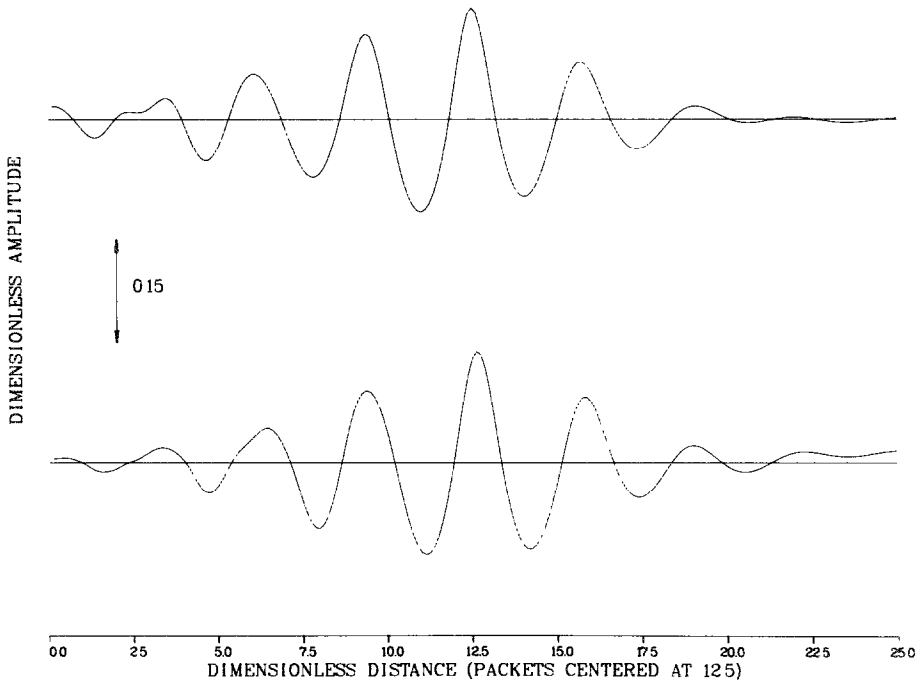

FIG. 12. Details of dispersive wave packet of Fig. 11. The upper profile is at $t = 50$: the lower profile is at $t = 25$.

profile (at $t = 25$). When large (the center of the figure), the waves are somewhat sharp-crested. From this we can conclude that the wave model reproduces the sharp-crested feature possessed by high water waves, even when the wavelength is not so long. Whether all features of high, not-so-long waves are reproduced from this long-wave model is not yet possible to say.

C. *Waves in Channels of Variable Breadth*

The wave model incorporates a variable channel breadth, under the circumstance that a measure of the length over which the breadth changes substantially is much greater than the horizontal scale of the wave. A computational channel was set up to replicate conditions of experiments by Chang *et al.* [31]. The channel is 10 times wider or narrower at one end than at the other. We connect the converging/diverging parts of the channel with parallel wall geometry, so that a wave can travel a long way before encountering the variable part of the channel. For the diverging case, parallel side walls occupy the region between $x = 0$ and $x = 120$. The walls then diverge from $x = 120$ to the end of the channel, which is at $x = 200$ (see the top of Fig. 15). The experiments had a shorter entrance section, and did not terminate in a rigid wall. Before the wave bounces off the end wall, however, the computations should mirror the experiments.

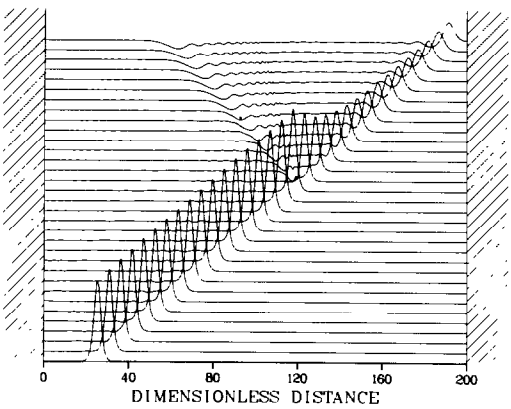

FIG. 13. Solitary wave propagating to and through a diverging channel (see top of Fig. 15 for the geometry). Again, the time scale is the same as the space scale, so that the time interval between profiles is 4.625. The elevation scale is 0.05 per interval; the initial waveform has a maximum of 0.4. Calculations are run with second-order dispersion and $\Delta x = \Delta t = 1/8$.

They do. Figure 13 displays the propagation of a wave that is designed to be a solitary wave initially, as in earlier displays. The initial conditions are set to be the same as those of the leftward-propagating wave of Fig. 10 (except that it is right-going), i.e., with an amplitude that stayed constant near 0.386 as the wave approached the entrance to the diverging part of the channel at $x = 120$. The wave generates a significant reflected wave as it first passes through the diverging section of the channel. It is here that reflections are expected to be the largest, for the nondimensional length associated with changes of channel breadth are the largest near the entrance section. The solitary wave gets smaller, and acquires an oscillatory

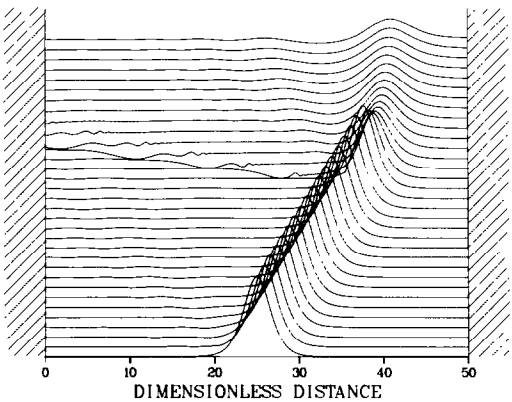

FIG. 14. Solitary wave propagating to and through a diverging channel. The data are the same as for Fig. 13, but are viewed from the coordinate system moving to the right with a dimensionless speed of unity, the coordinate systems being aligned at $t = 0$.

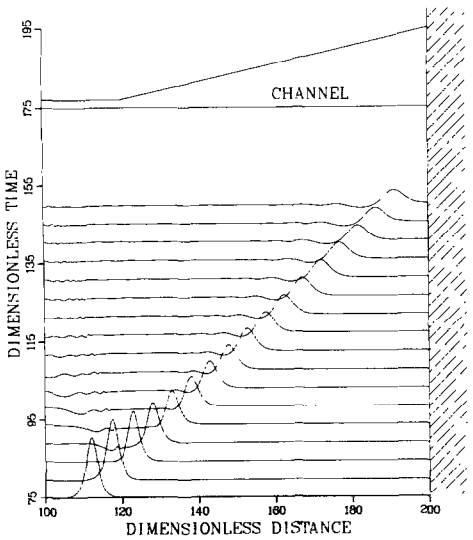

FIG. 15. Solitary wave propagating through a diverging channel. The data are the same as for Figs. 13–14, and clearly show the oscillatory tail that trails the lead wave. This tail is present in laboratory experiments, but not in a Korteweg–deVries theory.

tail. It also slows down; this is illustrated more clearly in Fig. 14, which uses the same data as for Fig. 13, but views the scene from the coordinate system which moves with the speed of the long wavelength limit of linear wave, $\sqrt{gh_0}$. The wave travels considerably faster than this limiting speed at first, and then slows down as it becomes weaker, still exceeding $\sqrt{gh_0}$. The propagation speed of the wave crest lies close to that of a solitary wave of the same amplitude. Figure 15 expands the view over the section in which Chang *et al.* performed experiments. They used wave probes to give a time history of elevation at one of several selected locations. They also compare their observations with a Korteweg–deVries theory. Witting and McDonald [23] compare their experiments with theories. Let it suffice to say that the theory given here reproduces the essential features of the experiment, such as the oscillatory tail behind the wave crest generated as the wave passes through the diverging section, while the Korteweg–deVries theory does not.

Figure 16 replicates conditions of another experiment of Chang *et al.* [31], this example showing waves in a converging channel. Because the physical still-water-depth happened to be different in this (converging channel) experiment from the previous (diverging channel) one, the dimensionless geometry is different. Here the channel entrance section extends to $x = 140$, and the 10-fold converging part occupies only the region between $x = 140$ and $x = 200$. The solitary wave gets bigger (and travels faster) as it propagates in the converging section. Dramatic reflected waves and oscillatory wave trains following the major disturbance are absent from this scene. There is a long positive tail to the wave, however, which is consistent with the

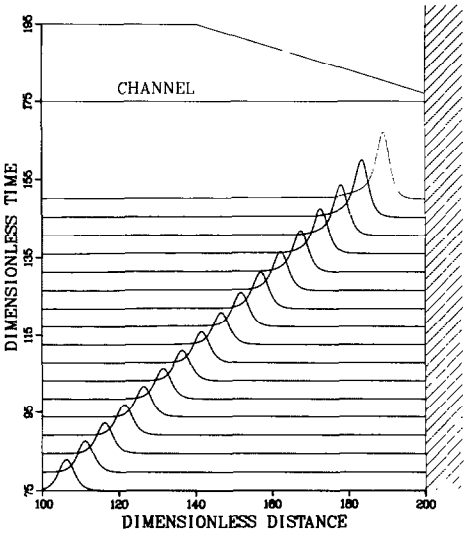

FIG. 16. Solitary wave propagating through a converging channel. The wave was launched at $t = 0$, $x = 25$, with an amplitude of 0.2. The elevation scale is 0.15 per interval. Calculations are run with second order dispersion and $\Delta x = \Delta t = 1/8$.

experiments, but inconsistent with Korteweg–deVries theory (see Witting and McDonald [23]).

Two asymptotic theories describe the behavior of waves in channels of gradually varying breadth: the first, derived by Green [26], predicts that the amplitude of the disturbance a is related to the channel breadth b by

$$a \propto b^{-1/2}. \tag{5.6}$$

The second, discussed in detail by Miles [32], who independently derives earlier results, gives

$$a \propto b^{-2/3}. \tag{5.7}$$

The first result *assumes* that the waves can be described by linear long wave theory, and that the disturbance is small compared to the distance over which the channel varies substantially. The second result *assumes* that the waves can be described by a Korteweg–deVries theory, and that the channel changes breadth so gradually that not only is there room for the wave itself, but also for the wave to continually reform itself so as to remain a solitary wave. The wave propagations shown in Figs. 13–16, and also from other geometries and initial conditions, give results that generally lie between the extremes of Eqs. (5.6)–(5.7), and cast doubts as to whether in practice the requirements of the asymptotic theories apply. Briefly, it appears that extremely long channels (L = hundreds) may be required to allow sufficiently gradual changes in breadth. For cases run in moderate-length channels ($L = 200$) there is not enough

room. Moreover, in situations where a channel has a converging/diverging section with entrance and exit sections identical, we find irreversible behavior; i.e., the emerging waves are smaller when they leave the variable section than they were when they entered. The calculations show that this is principally the result of reflected waves that escape to infinity whenever a wave passes through a section of variable breadth. Both asymptotic theories incorrectly predict reversibility, at least in the sense that the amplitude of the emerging wave should be identical to that of the entering wave.

D. *Undular Bores and Long Waves*

Computational experiments were run to see whether it would be possible to simulate the laboratory experiments of Favre [25], which, even today, form the most complete set. One aspect was not modeled—the manner by which the bores were generated. Favre pushed water into one end of his box; here a "dam" is broken, the water filling the computational region being initially still. Figure 17 simulates one of Favre's experiments (see his Fig. 41). The water at the left has a dimensionless height of 0.4. Two waves are launched from the initial condition: a long wave that travels to the left, unsteepens, and reflects from the wall at $x = 0$. This wave could just as well be described by long wave theory as by anything more sophisticated. The initially long wave travelling to the right, however, steepens for a while, and then starts to generate a wavetrain. The entire structure to the right of $x = 141$ is a bore that soon becomes undular, but never reaches a steady state. The maximum elevation of the undulations becomes about 0.4 at late times.

The experiments of Favre show the undulations to form at much earlier times, so calculations were performed with an initially sharper gradient of elevation. Figure 18

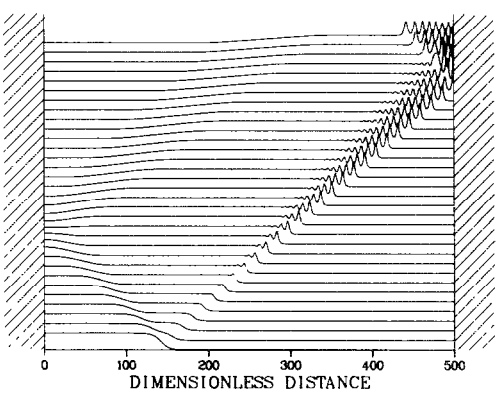

FIG. 17. Undular bore and long wave disturbance from the breaking of a gentle-faced dam. The time scale is the same as the space scale, so that the time interval between profiles is 11.5625. The elevation scale is 0.2 per interval; the initial elevation at the left is 0.4. The calculations are run with fourth-order dispersion and $\Delta x = \Delta t = 0.3125$.

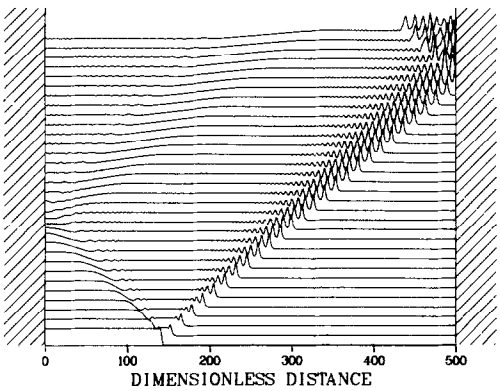

FIG. 18. Undular bore and other disturbances from the breaking of a sharp-faced dam. The time scale is the same as the space scale, so that the time interval between profiles is 11.5625. The elevation scale is 0.2 per interval; the initial elevation at the left is 0.4. The calculations are run with fourth-order dispersion and $\Delta x = \Delta t = 0.3125$.

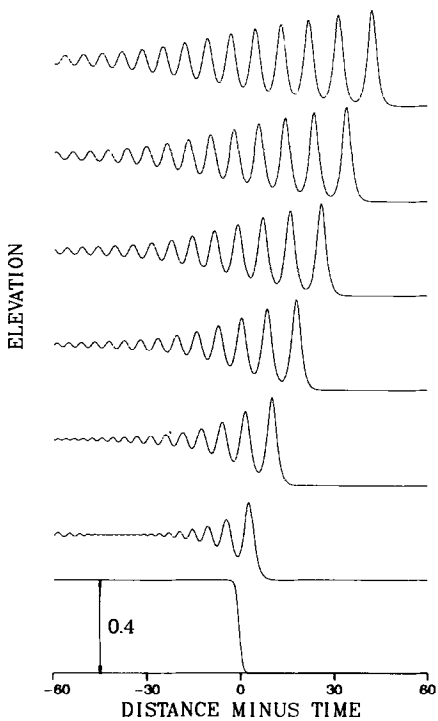

FIG. 19. Detailed view of an undular bore. The data are samples of the same data shown in Fig. 18, but are viewed from the coordinate system moving to the right with a dimensionless speed of unity, the coordinate systems being aligned at $t = 0$. Shown are the profiles at every 148th time step, and, from bottom to top, occur near $t = 0$, 46, 93, 139, 185, 231, and 278.

shows the results. The unsteepening wave of depression travelling to the left is now accompanied by an oscillatory wave train, generated, presumably, by the initial sharp gradient. The undular bore is qualitatively the same, but the undulations begin to form earlier. Indeed, the number of waves in the train at any time closely resembles the number in the wave probe records shown by Favre at locations comparable in space-time.

One interesting feature of the calculations, also seen earlier [33], is that the water depth at the location of the initial disturbance rapidly goes to the value given by long wave theory, until reflections from end walls intrude. For the conditions of Fig. 17 this is not surprising, for the wave is at least initially long. For the conditions of Fig. 18, assumptions of the long wave theory are violated even initially, and so the manner by which the system adjusts to the long wave results is an interesting problem. I have no idea how to go about deriving this observed result from analysis.

To see the undular bore structure a little better, the data of Fig. 18 are replotted from the frame of reference moving to the right with a speed of $\sqrt{gh_0}$. Plotted in Fig. 19 are the initial, 4th, 8th ... 24th profiles of Fig. 18. This corresponds to times of 46, 93, 139, 185, 231, and 278. The qualitative features correspond closely to

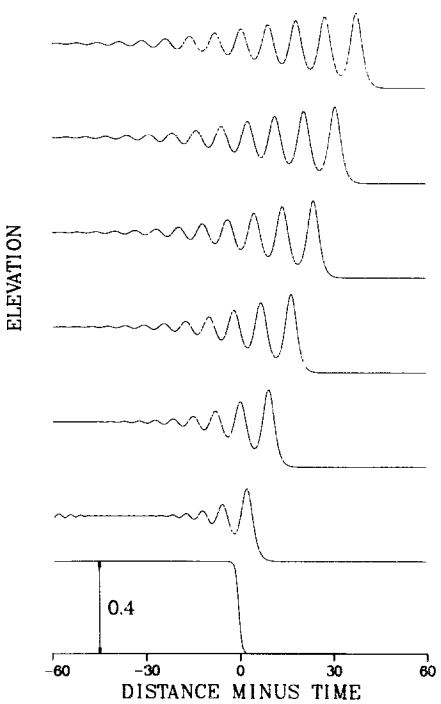

FIG. 20. Detailed view of an undular bore with dissipation. Initial data and running conditions are

calculations using the Korteweg–deVries equation (see Peregrine [11] and Vliegenthart [27]). For example, the line connecting particular crests near the front is nearly straight, its slope decreasing as time increases. Favre's experiments at early times show the same behavior. At late times, however, Favre's data show "saturation," the lead few waves having the same amplitude, only the waves further back showing the evolving sloping line. Thus, the results of the computations given here do not model this feature of the experiment any better than do other theories.

In an attempt to better model the experiments, some dissipation was added. The form of model dissipation is that of the trapezoidal correction of the basic leapfrog method, performed at each time step. Figure 20 shows the results for the same conditions as in Fig. 19. Figure 20 looks like a damped picture of Fig. 19, i.e., the waves are smaller, but the overall envelopes of the profiles are qualitatively the same. It is true that there are differences in the model dissipation and the laboratory dissipation. Nevertheless, it is likely that the difference between experiment and theory is due to something other than dissipation, perhaps surface tension. This contrasts with the case treated in the last subsection, where the experiments definitely favor this theory over Korteweg–deVries theory.

6. Discussion

The end result of the work reported here is a new model of water waves that can describe a wide variety of propagation situations accurately and efficiently. The following factors are responsible for this development:

1. The model uses exact prognostic equations in conservation form, Eqs. (2.4) and (2.5). A very general derivation of (2.5) is given by McDonald and Witting [24]. To my knowledge it has not been used in wave modeling before now.

2. Higher-order expansions than used before connect the velocity variables that appear in the governing equations. This allows the model (a) to incorporate long wave theory exactly, (b) to give a good representation of waves all the way out to kh_0 exceeding 8, thus including both shallow water and essentially deep water waves in the same model, and (c) to represent fairly-long nonlinear waves to one order better than Boussinesq.

3. The model employs a numerical method, i.e., pure leapfrog, that gives no unwanted numerical diffusion. The time-stepping procedures are simple enough to analyze in some detail and to implement efficiently on vector computers.

4. The model takes a time step equal to a space step (in nondimensional units for which the linear long wave speed is unity). This allows for efficient machine computations, unlike methods developed for the Korteweg–deVries equation. Moreover, this procedure removes any spurious numerical dispersion at order $k^2(\Delta x)^2$.

5. Finally, the diagnostic equations are cast in a form such that only tri-

diagonal matrix equations need to be solved. A very fast, fully vectorized algorithm is then used to invert the matrices [34].

Running times for the unified waves model on the TI–ASC–7 computer are approximately 20 msec per time step for a computational region containing 1600 grid points. A run to $t = 150$ with resolution $\Delta x = \Delta t = 1/8$ takes about 24 sec. About half of the running time is spent in collecting diagnostic information and can be eliminated, if desired. In summary, computer costs to run the model are very small.

No detailed comparisons have been made with other numerical models for specific problems. In general, though, it is clear from Figs. 2–6 that the model is considerably more accurate than Boussinesq models, and can deal with higher and shorter waves. The flexibility of the model to treat different physical conditions is illustrated by Figs. 7–20 with accompanying text. Consequently, the model represents a great improvement over other expansion-type models. Except for breaking waves and other extreme situations that it cannot reach, the unified waves model can treat the same problems as non-expansion-type models, such as Lagrangian and Marker-in-cell models, but at a tiny fraction of the cost. In practice, these more complicated models do not employ a resolution fine enough to compete with the new waves model.

ACKNOWLEDGMENTS

The author thanks Dr. B. E. McDonald for many valuable discussions during the course of the research. The work was supported by the Coastal Sciences Group, Ocean Sciences Division, Office of Naval Research.

REFERENCES

1. H. LAMB, "Hydrodynamics," 6th ed., Cambridge Univ. Press, Cambridge, 1932; reprinted, Dover, New York, 1945.
2. J. J. STOKER, "Water Waves," Interscience, New York, 1957.
3. J. S. RUSSELL, *in* "Report, Meeting Brit. Assoc. Adv. Sci., 7th Liverpool, 1837," pp. 417–496, London, Murray, 1838.
4. J. S. RUSSELL, *in* "Report, Meeting Brit. Assoc. Adv. Sci. 14th York, 1844," pp. 311–390, London, Murray, 1845.
5. M. J. BOUSSINESQ, *J. Math. Pures Appl.* **17** (1872), 55–108.
6. M. J. BOUSSINESQ, *C. R. Acad. Sci. Paris* **72**(1871), 755–759.
7. D. J. KORTEWEG AND G. DEVRIES, *Philos. Mag. Ser. 5* **39** (1895), 422–443.
8. N. J. ZABUSKY AND M. D. KRUSKAL, *Phys. Rev. Lett.* **15** (1965), 240–243.
9. N. J. ZABUSKY, *J. Comput. Phys.* **43** (1981), 195–249.
10. A. T. CHWANG AND T. Y. WU, *in* "Proceedings, IUTAM Symposium on Water Waves of Varying Depth," Canberra, Australia, 1976.
11. D. H. PEREGRINE, *J. Fluid Mech.* **25** (1966), 321–330.
12. D. H. PEREGRINE, *J. Fluid Mech.* **27** (1967), 815–827.
13. O. S. MADSEN AND C. C. MEI, *J. Fluid Mech.* **39** (1969), 781–791.
14. M. B. ABBOTT, H. M. PETERSEN, AND O. SKOVGAARD, *J. Hydraulic Res.* **16** (1978), 173–204.

15. D. R. Basco, "Surf Zone Currents," Miscellaneous Report No. 82–7, U. S. Army Corp of Engineers, Coast. Engr. Res. Center, Sept. 1982.
16. F. H. Harlow and A. A. Amsden, "Fluid Dynamics," Los Alamos Scientific Lab. LA–4700, 1971.
17. R. K. Chan and R. L. Street, *J. Comput. Phys.* **6** (1970), 68–94.
18. M. J. Fritts and J. P. Boris, *J. Comput. Phys.* **31** (1979), 173–215.
19. J. D. Fenton and M. M. Rienecker, *J. Fluid Mech.* **118** (1982), 411–443.
20. M. S. Longuet–Higgins and E. D. Cokelet, *Proc. Roy. Soc. London Ser. A* **350** (1976), 1–26; **364** (1978), 1–28.
21. M. S. Longuet–Higgins and J. D. Fenton, *Proc. Roy. Soc. London Ser. A* **340** (1974), 471–493.
22. J. M. Witting, "High Solitary Waves in Water: Results of Calculations," NRL Formal Report 8505, 1981.
23. J. M. Witting and B. E. McDonald, "A Conservation-of-Velocity Law for Inviscid Fluids," NRL Memorandum Report 4977, 1982.
24. B. E. McDonald and J. M. Witting, *J. Comput. Phys.* **56** (1984), 203–236.
25. H. Favre, "Étude théorique et expérimentale des ondes de translation dans les canaux découverts," Paris, Dunod, 1935.
26. G. Green, *Cambridge Philos. Trans.* **6** (1838), 457–462.
27. A. C. Vliegenthart, *J. Engrg. Math.* **5** (1971), 137–155.
28. J. L. Bona, W. G. Pritchard, and L. R. Scott, *Phys. Fluids* **23** (1980), 438–441.
29. A. R. Santarelli, *Nuovo Cimento B* **46** (1978), 179–180.
30. J. C. Lewis and J. A. Tjon, *Phys. Lett. A* **73**(1979), 275–279.
31. P. Chang, W. K. Melville, and J. W. Miles, *J. Fluid Mech.* **95** (1979), 401–414.
32. J. W. Miles, *J. Fluid Mech.* **91** (1979), 181–190.
33. J. Witting, *SIAM J. Appl. Math.* **28** (1975), 700–719.
34. J. P. Boris, "Vectorized Tridiagonal Solvers," NRL Memorandum Report 3408, 1976.